Supporting Information

Rediscovery of nylon upgraded by interactive biorenewable nanofillers

Lam Tan Hao,‡[a,b] Youngho Eom,‡[a,c] Thang Hong Tran,[a,b] Jun Mo Koo,[a] Jonggeon Jegal,[a] Sung Yeon Hwang,*[a,b] Dongyeop X. Oh*[a,b] and Jeyoung Park*[a,b]

[a] *Research Center for Bio-based Chemistry, Korea Research Institute of Chemical Technology (KRICT), Ulsan 44429, Republic of Korea. E-mail: crew75@krict.re.kr, dongyeop@krict.re.kr, jypark@krict.re.kr*

[b] *Advanced Materials and Chemical Engineering, University of Science and Technology (UST), Daejeon 34113, Republic of Korea*

[c] *Department of Polymer Engineering, Pukyong National University, Busan, 48513, Republic of Korea*

‡ These authors contributed equally.

* Corresponding authors

s 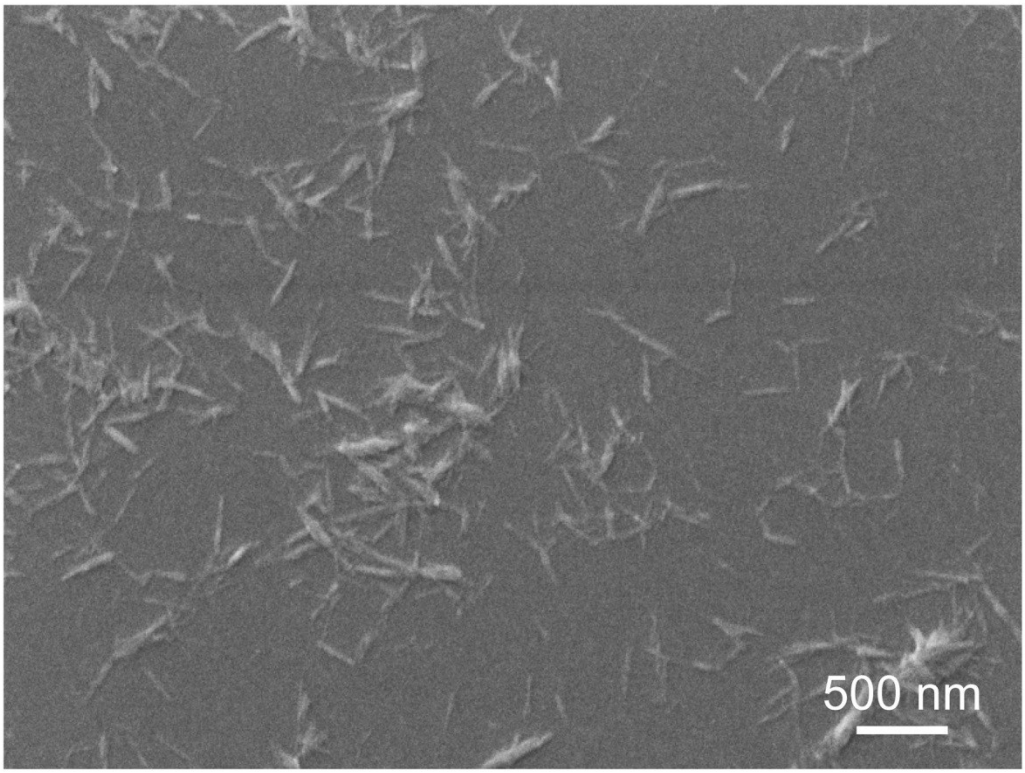

Fig. S1 Scanning electron microscope (SEM) image of chitosan nanowhisker (CSW).

The average size range of CSW was determined by measuring the diameter and length of 100 random whiskers using SEM. The diameter was measured to be in the 10–25 nm range, and the length was measured to be in the 150–250 nm range. Furthermore, the length of CSW based on the hydrodynamic diameter of an equivalent sphere was measured to be 228.1 nm (with a zeta potential of +43.3 mV at pH 4) using the zeta sizer (Nano ZS, Malvern, UK).

Table S1 Preparation, molecular weight, and thermal properties of nylon 66 nanocomposites.

Nanofiller content (wt%)	Sample code	M_V [a] (g mol^{-1})	T_{d5} [b] (°C)	T_{max} [c] (°C)	T_c [d] (°C)
0.0 (neat)	Ny66	33,500	359	408	229
In situ nylon 66/CNC[e] composites					
0.1	I-NC0.1	30,800	365	412	232
0.2	I-NC0.2	30,100	363	411	233
0.3	I-NC0.3	33,900	363	416	234
0.4	I-NC0.4	30,900	380	421	236
0.5	I-NC0.5	27,800	371	415	238
In situ nylon 66/CSW[f] composites					
0.1	I-NS0.1	29,400	367	424	233
0.2	I-NS0.2	30,900	372	426	235
0.3	I-NS0.3	31,100	378	433	234
0.4	I-NS0.4	29,000	371	423	235
0.5	I-NS0.5	32,000	-	-	-
Solution-blended nylon 66/CNC composites					
0.1	B-NC0.1	33,500	371	412	231
0.2	B-NC0.2		364	412	232
0.3	B-NC0.3		364	414	234
0.4	B-NC0.4		365	408	234
0.5	B-NC0.5		370	415	233
Solution-blended nylon 66/CSW composites					
0.1	B-NS0.1	33,500	371	422	232
0.2	B-NS0.2		384	436	233
0.3	B-NS0.3		379	436	233
0.4	B-NS0.4		379	451	234
0.5	B-NS0.5		378	460	234

[a]Viscosity average molecular weight. [b]Degradation temperature at 5% weight loss. [c]Degradation temperature at maximum weight loss. [d]Crystallization temperature. [e]Cellulose nanocrystal. [f]Chitosan nanowhisker.

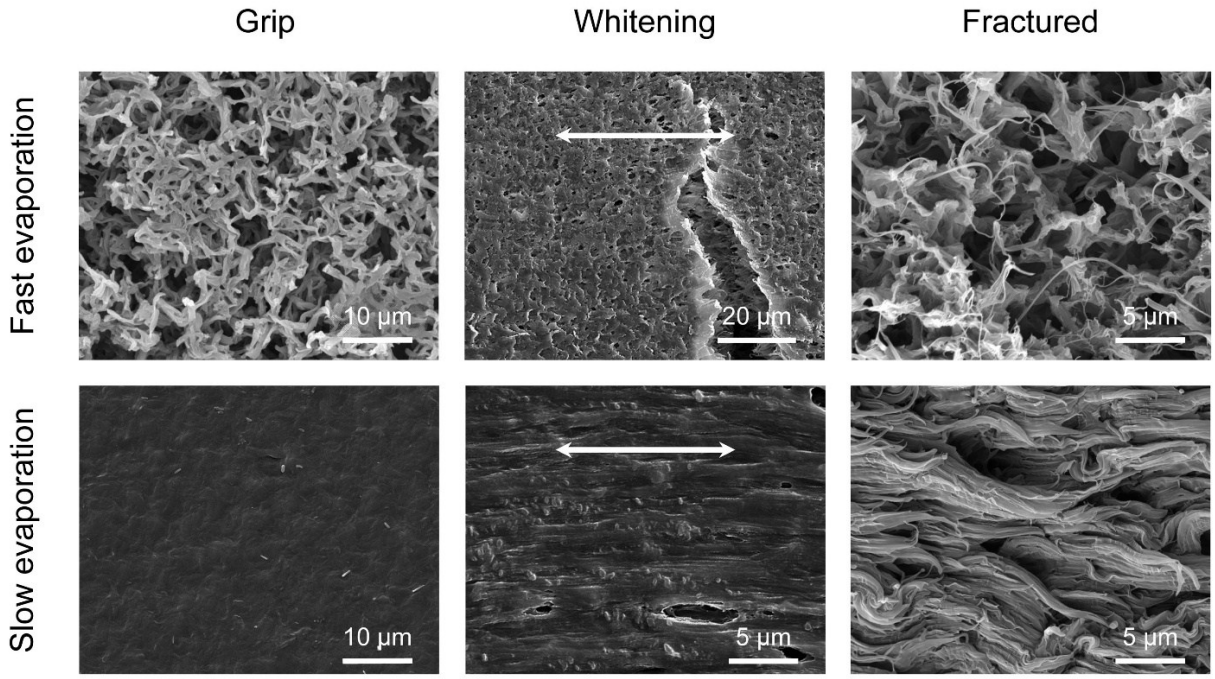

Fig. S2 SEM images of executed dumbbell-shaped test specimens, which show the difference in morphology at the grip, whitening (necking), and fractured cross-section positions of neat nylon films obtained from fast and slow evaporation of formic acid. White arrows indicate the tensile force direction.

In Fig. S2, SEM images of representative tensile specimens of the two films are shown. The fast-evaporated film is denoted by F_Ny66, and the slow-evaporated film is denoted by Ny66. The surface of the F_Ny66 film was highly porous, and the sizes of the macropores ranged ~3–7 μm. In contrast, the Ny66 film displayed a continuous surface. Investigation of the tensile-induced whitening deformation area and the fractured surface provided further information on the arrangement of nylon fibers in the two samples. The F_Ny66 tensile specimen showed the formation of large cracks, which were noticeable in the whitening region. Furthermore, the polymer fibers were randomly entangled with each other, as revealed in the fractured surface. However, the Ny66 sample showed a regular alignment of nylon fibers stretched along the tensile axis. It is speculated that the rapid evaporation of solvents during film formation did not provide sufficient time for the rearrangement and assembly of the nylon 66 strands in an ordered fashion.

Table S2 Tensile properties of nylon 66 nanocomposites.

Sample code[a]	Young's modulus (*E*, GPa)	Ultimate tensile strength (σ, MPa)	Elongation at break (ε_b, %)	Toughness (U, MJ m^{-3})
Ny	1.4 ± 0.1	61 ± 3.6	93 ± 4.5	50 ± 2.8
C_Ny[b]	1.6 ± 0.1	67 ± 2.3	99 ± 10	54 ± 5.1
In situ nylon 66/CNC composites				
I-NC0.1	1.5 ± 0.1	69 ± 4.2	86 ± 4.3	54 ± 3.1
I-NC0.2	1.8 ± 0.1	76 ± 2.2	64 ± 3.7	41 ± 3.8
I-NC0.3	2.0 ± 0.1	89 ± 3.4	59 ± 3.0	41 ± 1.9
I-NC0.4	2.2 ± 0.1	100 ± 5.2	48 ± 3.4	39 ± 3.3
I-NC0.5	2.1 ± 0.2	89 ± 7.6	39 ± 3.3	30 ± 4.3
In situ nylon 66/CSW composites				
I-NS0.1	1.6 ± 0.1	76 ± 7.1	39 ± 14	26 ± 9.7
I-NS0.2	1.9 ± 0.1	78 ± 3.3	24 ± 9.6	18 ± 9.0
I-NS0.3	2.6 ± 0.1	97 ± 3.2	27 ± 6.5	23 ± 6.2
I-NS0.4	2.6 ± 0.0	106 ± 2.0	30 ± 3.0	28 ± 4.1
I-NS0.5	-	-	-	-
Solution-blended nylon 66/CNC composites				
B-NC0.1	1.5 ± 0.1	70 ± 4.2	78 ± 4.3	49 ± 2.6
B-NC0.2	1.6 ± 0.1	73 ± 5.6	79 ± 4.9	47 ± 5.2
B-NC0.3	1.6 ± 0.1	74 ± 2.5	75 ± 4.4	45 ± 3.7
B-NC0.4	2.0 ± 0.1	86 ± 4.4	63 ± 8.2	47 ± 15
B-NC0.5	1.9 ± 0.1	85 ± 4.9	64 ± 6.2	42 ± 5.7

Sample code[a]	Young's modulus (*E*, GPa)	Ultimate tensile strength (σ, MPa)	Elongation at break (ε_b, %)	Toughness (U, MJ m^{-3})
Solution-blended nylon 66/CSW composites				
B-NS0.1	1.4 ± 0.1	72 ± 2.8	127 ± 29	78 ± 17
B-NS0.2	1.6 ± 0.2	72 ± 4.7	140 ± 22	89 ± 17
B-NS0.3	1.7 ± 0.0	78 ± 3.4	147 ± 30	104 ± 22
B-NS0.4	1.8 ± 0.1	80 ± 1.4	100 ± 34	71 ± 23
B-NS0.5	2.2 ± 0.0	87 ± 3.0	94 ± 16	75 ± 13

[a]Refer to Table S1 for the sample codes. [b]Commercial nylon 66 sourced from Sigma-Aldrich. Data are displayed as means ± standard deviations of at least five specimens tested.

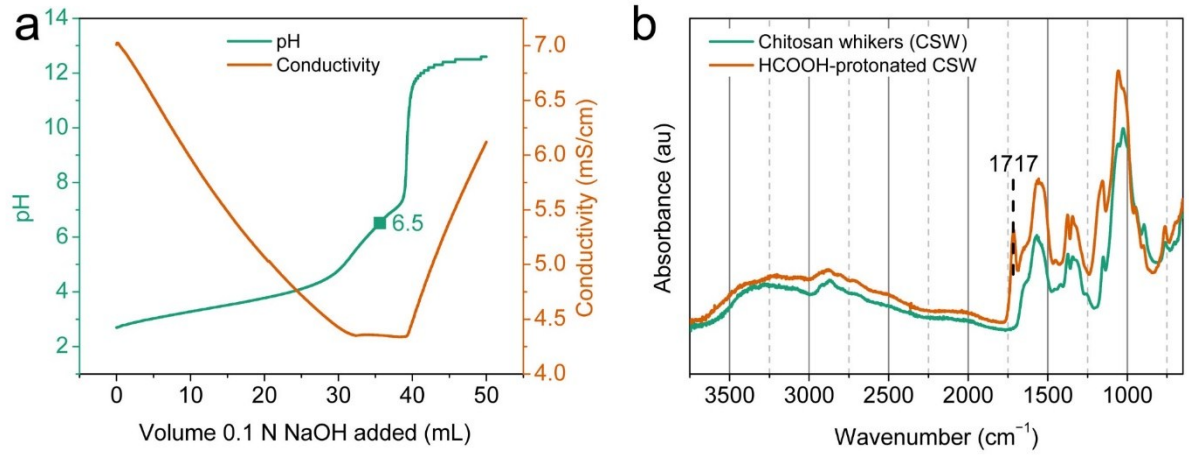

Fig. S3 Protonation of CSW with formic acid (HCOOH). (a) Titration curves of CSW protonated with formic acid solution (0.1 N, pKa = 3.75). (b) Fourier transformed-infrared (FTIR) spectra of CSW films casted from solvent evaporation of deionized water (pH 7.0) and formic acid.

1. Preparation of an acidified CSW suspension

CSW (300 mg) were dispersed in deionized water (40 mL) by homogenization at 5000 rpm using a homogenizer (T 25 ULTRA-TURRAX®, IKA, Germany) for 10 min. The mixture was sonicated at 50% amplitude for 30 min at 25 °C using an Ultrasonic Cleaner (SD-D400H, LKLABKOREA Inc., Korea). After that, formic acid (150 µL, Sigma Aldrich, 96%) was added to the resulting suspension under magnetic stirring for 24 h to ensure complete protonation of CSW. The concentration of formic acid in the suspension was ~0.1 N. The initial pH (before titration) of the suspension was 2.64, at which virtually all $–NH_2$ groups (pKa 6.5) of CSW were protonated. The initial conductivity was measured to be 7.010 mS cm^{-1} using the 912 conductometer (Metrohm, Switzerland), which indicated the dominance of H^+.

2. Titration of the CSW suspension with NaOH

A solution of NaOH (50 mL, 0.1 N, Sigma Aldrich) was added to the CSW suspension at a flow rate of 0.05 mL min^{-1} using a syringe pump (GELATO, KD Scientific, US). The pH and the conductivity of the suspension were recorded at 30-s intervals and were plotted against the volume of NaOH solution added.

Fig. S3a shows the titration results, where a typical conductometric titration curve of an acidic chitosan dispersion was obtained. The lower segment of the curve is attributed to the neutralization of the protonated amino groups present in CSW.[1] Its midpoint is well-matched with the pKa value (6.5) of chitosan NH_2 (ref.2) that specifies the half-equivalence point on the pH-metric curve.

Pristine films of CSW were prepared by casting in formic acid under a slow solvent evaporation rate and then their attenuated total reflectance Fourier-transformed infrared (ATR-FTIR) spectrum was obtained and was compared with the one acquired for a CSW film casted from water (Fig. S3b). The appearance of the peak at 1717 cm^{-1}, which is characteristic of the formic acid's C=O stretching, in the formic acid-casted film indicated the protonation of the CSW's surface amino groups. Ionic interactions between NH_3^+ and COO^- would reduce the hydrogen bonding capability of CSW with the nylon matrix, which resulted in a weaker matrix-filler interaction that led to a lower *E* and a higher ε_b of the B-NS series, compared to the other composites.

Table S3 Comparison of the ultimate tensile strength (σ) and elongation at break (ε_b) of polyamide (nylon) nanocomposites in this study with reported polyamide composites.

Filler (natural organic nanofillers)	Polyamide (PA)	Processing	Ultimate tensile strength (σ)					Elongation at break (ε_b)					Ref.
			Filler content (wt%)	σ of neat PA (MPa)	σ of PA composite (MPa)	σ increase (fold)	σ increase per unit filler loading [(fold−1) wt%$^{-1}$]	Filler content (wt%)	ε_b of pristine PA (%)	ε_b of PA composites (%)	ε_b increase (fold)	ε_b increase per unit filler loading [(fold−1) wt%$^{-1}$]	
CNC[a]	PA66	Solution casting	0.4	61	100	1.64	1.60	0.4	93	48	0.52	−1.2	This work
CNC[b]			0.4	61	86	1.41	1.03	0.4	93	63	0.68	−0.8	
CSW[a]			0.4	61	106	1.74	1.85	0.4	93	30	0.32	−1.7	
CSW[b]			0.5	61	87	1.43	0.86	0.3	93	147	1.6	1.9	

[a]*In situ* polymerized PA66 nanocomposites. [b]Solution-blended PA66 nanocomposites.

Table S3 Comparison of ultimate tensile strength (σ) and elongation at break (ε_b) of polyamide nanocomposites in this study with other previous reported polyamide composites *(continued)*.

Filler (natural organic fillers)	Polyamide (PA)	Processing	Ultimate tensile strength (σ)					Elongation at break (ε_b)					Ref.
			Filler content (wt%)	σ of neat PA (MPa)	σ of PA composite (MPa)	σ increase (fold)	σ increase per unit filler loading [(fold−1) wt%$^{-1}$]	Filler content (wt%)	ε_b of pristine PA (%)	ε_b of PA composites (%)	ε_b increase (fold)	ε_b increase per unit filler loading [(fold−1) wt%$^{-1}$]	
Cellulose whiskers[c]	PA6	Injection	1.0	54	50	0.93	−0.07	1.0	60	33	0.55	−0.45	3
Coated cellulose whiskers[d]			1.0	54	52	0.96	−0.04	1.0	60	73	1.22	0.22	
Nanocrystalline cellulose[e]			3.0	67	74	1.1	0.03	3.0	336	55	0.16	−0.28	4
Coconut shell particles[f]			15	70	77	1.1	0.01	No data					5
ECO Bright fibers[g]			30	72	118	1.64	0.02	No data					6
TerraCel™ [h]			30	72	120	1.67	0.02	No data					
Stone groundwood fibers[i]	PA11		50	38	64	1.67	0.01	50	25	3.7	0.15	−0.02	7

[c]Obtained from commercial cotton fibers through acid hydrolysis using H_2SO_4. [d]Coated with PA6 by dissolving in formic acid followed by solvent evaporation. [e]Produced by acid hydrolysis of a commercial bleached softwood Kraft pulp. [f]Contains 49.8% cellulose and 25.1% lignin. [g]Softwood wood pulp containing 90–100% cellulose. [h]Hardwood wood pulp containing 97–100% cellulose. [i]From softwood (*Pinus radiata*).

Table S3 Comparison of ultimate tensile strength (σ) and elongation at break (ε_b) of polyamide nanocomposites in this study with other previous reported polyamide composites *(continued)*.

Filler (carbon-based materials)	Polyamide (PA)	Processing	Ultimate tensile strength (σ)					Elongation at break (ε_b)					Ref.
			Filler content (wt%)	σ of neat PA (MPa)	σ of PA composite (MPa)	σ increase (fold)	σ increase per unit filler loading [(fold−1) wt%$^{-1}$]	Filler content (wt%)	ε_b of pristine PA (%)	ε_b of PA composites (%)	ε_b increase (fold)	ε_b increase per unit filler loading [(fold−1) wt%$^{-1}$]	
Graphene[j]	PA66	Solution casting	1.0	22	33	1.5	0.5	1.0	40	33	0.83	−0.18	8
Graphene[k]	PA6		3.0	68	109	1.60	0.20	3.0	75	45	0.6	−0.13	9
Graphene oxide (GO)[l]			1.0	51	96	1.88	0.88	1.0	27	13	0.48	−0.52	10
Reduced GO[m]	PA12	Hot-pressed	4.0	52	43	0.82	−0.04	4.0	254	6.8	0.03	−0.24	11
Multi-walled carbon nanotubes (MWNT)	PA610		1.5	36	51	1.43	0.29	1.5	10	13	1.3	0.2	12
	PA66		0.5	53	65	1.23	0.45	0.5	11	8.5	0.77	−0.45	13
Functionalized MWNT[n]			0.5	53	75	1.42	0.84	0.5	11	9	0.82	−0.36	
MWNT[o]	PA6	Injection	1.0	62	59	0.95	−0.05	1.0	235	133	0.57	−0.43	14
Functionalized MWNT[p]		Hot-pressed	1.0	18	40	2.24	1.24	1.0	>150	125	<0.83	<−0.17	15
Single walled carbon nanotubes (SWNT)			1.5	66	50	0.76	−0.16	1.5	350	68	0.19	−0.54	16
SWNT[q]			1.5	66	50	0.76	−0.16	2.5	350	307	0.88	−0.05	
SWNT	PA610	Melt spinning	1.0	67	79	1.18	0.18	1.0	440	262	0.60	−0.40	17
Functionalized			1.0	67	168	2.51	1.51	1.0	440	290	0.66	−0.34	

Filler (carbon-based materials)	Polyamide (PA)	Processing	Ultimate tensile strength (σ)					Elongation at break (ε_b)					Ref.
			Filler content (wt%)	σ of neat PA (MPa)	σ of PA composite (MPa)	σ increase (fold)	σ increase per unit filler loading [(fold−1) wt%$^{-1}$]	Filler content (wt%)	ε_b of pristine PA (%)	ε_b of PA composites (%)	ε_b increase (fold)	ε_b increase per unit filler loading [(fold−1) wt%$^{-1}$]	
SWNT[r]			1.0	67	177	2.64	1.64	1.0	440	368	0.84	−0.16	
Carbon fiber	PA6	Injection	20	52	111	2.15	0.06	20	276	3.4	0.01	−0.05	18

[j]Oxygen content is less than 1%. [k]Synthesized from graphene-ZnO composites by treatment with concentrated HCl solution. [l]Prepared from graphite using a modified Hummers and Offeman's method. Oxidizing agents used were $NaNO_3$, H_2SO_4, $KMnO_4$, and H_2O_2. [m]Prepared through thermal treatment of GO surface. The GO was prepared from graphite by modified Hummers' method using H_2SO_4 and $KMnO_4$ as oxidizing agents. [n]Amination using hexamethylenediamine. [o]Encapsulated with poly(*n*-butylacrylate). [p]Synthesized by catalytic chemical vapor deposition of methane on Co-Mo/MgO catalysts and functionalized by oxidation with 2.6 M HNO_3 solution. [q]Modified with styrene-maleic anhydride. [r]Functionalized with long-chain carboxylic acid groups, $–(CH2)_n–COOH$ (n = 4 and 9).

Table S3 Comparison of ultimate tensile strength (σ) and elongation at break (ε_b) of polyamide nanocomposites in this study with other previous reported polyamide composites *(continued)*.

Filler (Clays and others filler types)	Polyamide (PA)	Processing	Ultimate tensile strength (σ)					Elongation at break (ε_b)					Ref.
			Filler content (wt%)	σ of neat PA (MPa)	σ of PA composite (MPa)	σ increase (fold)	σ increase per unit filler loading [(fold−1) wt%$^{-1}$]	Filler content (wt%)	ε_b of pristine PA (%)	ε_b of PA composites (%)	ε_b increase (fold)	ε_b increase per unit filler loading [(fold−1) wt%$^{-1}$]	
Organoclay, Nanomer® I.34TCN[s]	PA66	Injection	5.0	73	83	1.14	0.03	No data					19
Cloisite 30B[t]	PA6	Melt extrusion	5.0	28	36	1.29	0.06	No data					20
Natural clay		Injection	8.0	66	76	1.15	0.02	No data					21
Halloysite A[u]			2.0	72	80	1.12	0.06	2.0	99	186	1.9	0.44	22
Montmorillonite clay (M1030D)			3.0	52	74	1.42	0.14	3.0	276	3.9	0.01	−0.33	18
Halloysite[v]	PA11		6.0	44	54	1.24	0.04	6.0	254	235	0.93	−0.01	23
Nano-SiO_2 [w]	PA66		3.0	72	79	1.10	0.03	No data					24
Glass fiber[x]	PA6		30	52	96	1.85	0.03	30	276	5.6	0.02	−0.03	18
Glass fibers/Montmorillonite clay (M1030D)[y]			30	52	107	2.06	0.04	30	276	2.4	0.009	−0.03	18

[s]Surface modified Montmorillonite mineral with a mean particle size of 16–22 μm. [t]Natural Montmorillonite-layered silicate modified with a ternary ammonium salt. [u]Tubular form with a cation exchange capacity of around 10 meq/g. [v]Average diameter of 80 nm, length of about 1.2 μm, and density of 2.5 g cm^{-3}. [w]Obtained using sodium metasilicate as the monomer, silane coupling agent as a chain terminator, and 3-aminopropyltriethoxysilane as a surface modifier. [x]6 mm long. [y]Glass fibers content: 30 wt.%; Clay content: 3 wt.

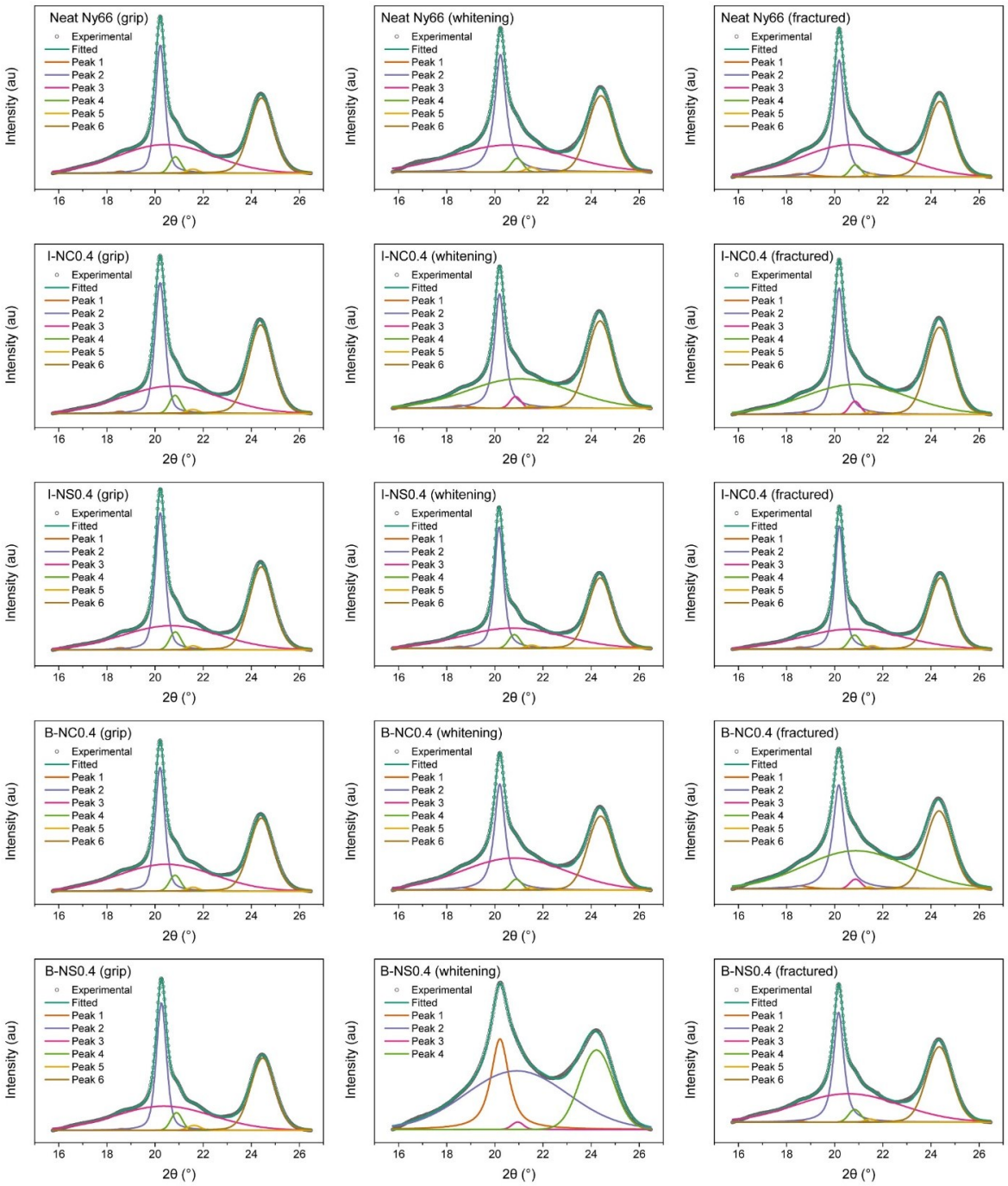

Fig. S4 1D WAXS patterns and peak deconvolution of (from top row to bottom row) neat Ny66, I-NC0.4, I-NS0.4, B-NC0.4, and B-NS0.4 films at filler loading of 0.4 wt% at (from left to right) grip, whitening (necking), and fractured cross-section positions.

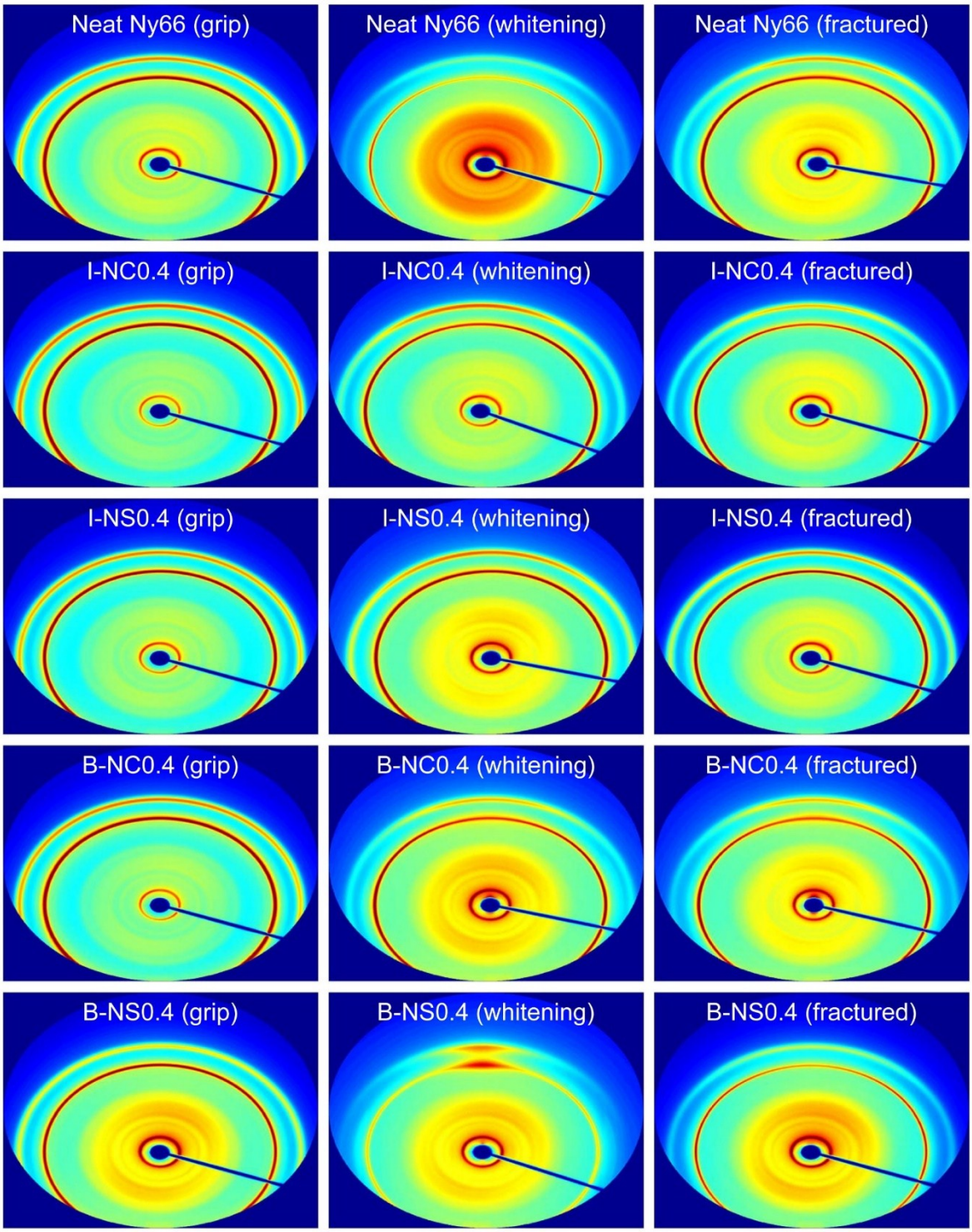

Fig. S5 2D WAXS patterns of (from top row to bottom row) neat Ny66, I-NC0.4, I-NS0.4, B-NC0.4, and B-NS0.4 films at filler loading of 0.4 wt% at (from left to right) grip, whitening (necking), and fractured cross-section positions.

Table S4 FTIR spectral band assignments of nylon 66 nanocomposites.

Wavenumbers (cm^{-1})	**Assignments**	**Refs.**
1631	Amide I (mainly C=O stretching of hydrogen-bonded C=O groups, in plane NH deformation, and possibly CN stretching)	25–28
1623–1611	Shifting of amide I due to an increase in hydrogen bonding	
1534	Amide II (mainly in-plane N–H bending of hydrogen-bonded N–H groups, CO stretching, and CN stretching)	25–28
1531–1521	Shifting of amide II due to an increase in hydrogen bonding	
1473	NH-vicinal CH_2 scissoring, *trans* conformation, regularity	26, 29
	Crystallinity	30
1466	All NH-non-vicinal CH_2 scissoring	26, 29
1438	Coincidence of NH-vicinal and CO-vicinal CH_2 scissoring	26, 29
1417	CO-vicinal CH_2 scissoring, *trans* conformation, regularity	26, 29
1371	Amide III (CN stretch, in plane NH deformation), coupled with hydrocarbon skeleton	25, 26
	CH_3 end group symmetric deformation	26
1332	Regular-folded chains	25, 26
	Crystallinity (Brill band)	31–33
1307	CH_2 twisting	26
1278	Amide III (CN stretch, in plane NH deformation), coupled with hydrocarbon skeleton	25, 26
1226	Regular-folded chains	26, 31, 32
1200	Amide III (CN stretch, in plane NH deformation), coupled with hydrocarbon skeleton	25, 26
	Crystallinity	30, 32–35
1060; 1070	Crystallinity	33
	Regularity	30
1040; 1013	Crystallinity (Brill bands)	33
937	Crystallinity	30, 34–36
907	(Possible) crystallinity	30, 34, 35

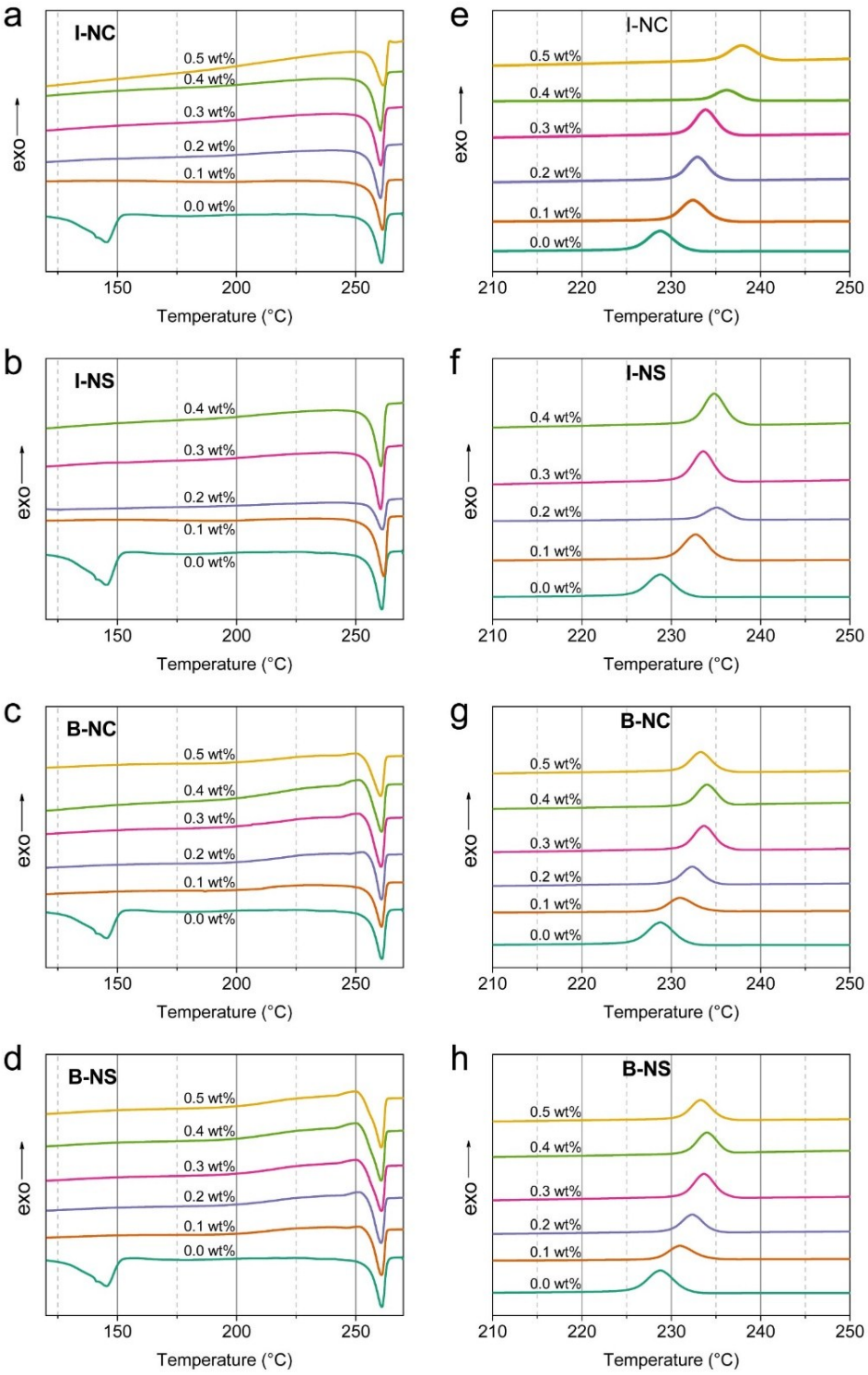

Fig. S6 Differential scanning calorimetry (DSC) thermograms showing the 1st heating run of (a) *in situ* Ny66/CNC (I-NC), (b) *in situ* Ny66/CSW (I-NS), (c) solution-blended Ny66/CNC (B-NC), and (d) solution-blended Ny66/CSW (B-NS) nanocomposite films. DSC thermograms showing the cooling runs of (e) I-NC, (f) I-NS, (g) B-NC, and (h) B-NS nanocomposite films.

Table S5 Crystallinity of nylon 66 nanocomposites based on heat of melting obtained from the first heating of differential scanning calorimetric data.

Sample code[a]	Heat of melting[b] (ΔH_m, J g^{-1})	Crystallinity X (%)
Ny66	54.90	29.14
I-NC0.1	62.08	32.95
I-NC0.2	63.80	33.86
I-NC0.3	63.92	33.93
I-NC0.4	63.41	33.66
I-NC0.5	64.76	34.37
I-NS0.1	63.81	33.87
I-NS0.2	61.07	32.42
I-NS0.3	61.47	32.63
I-NS0.4	62.39	33.12
B-NC0.1	71.11	37.74
B-NC0.2	69.49	36.88
B-NC0.3	68.94	36.59
B-NC0.4	72.29	38.37
B-NC0.5	69.71	37.00
B-NS0.1	70.07	37.19
B-NS0.2	71.83	38.13
B-NS0.3	69.20	36.73
B-NS0.4	71.11	37.74
B-NS0.5	70.20	37.26

[a]Refer to Table S1. [b]The heat of melting of theoretically crystalline nylon 66 is 188.4 J g^{-1}. (ref.37)

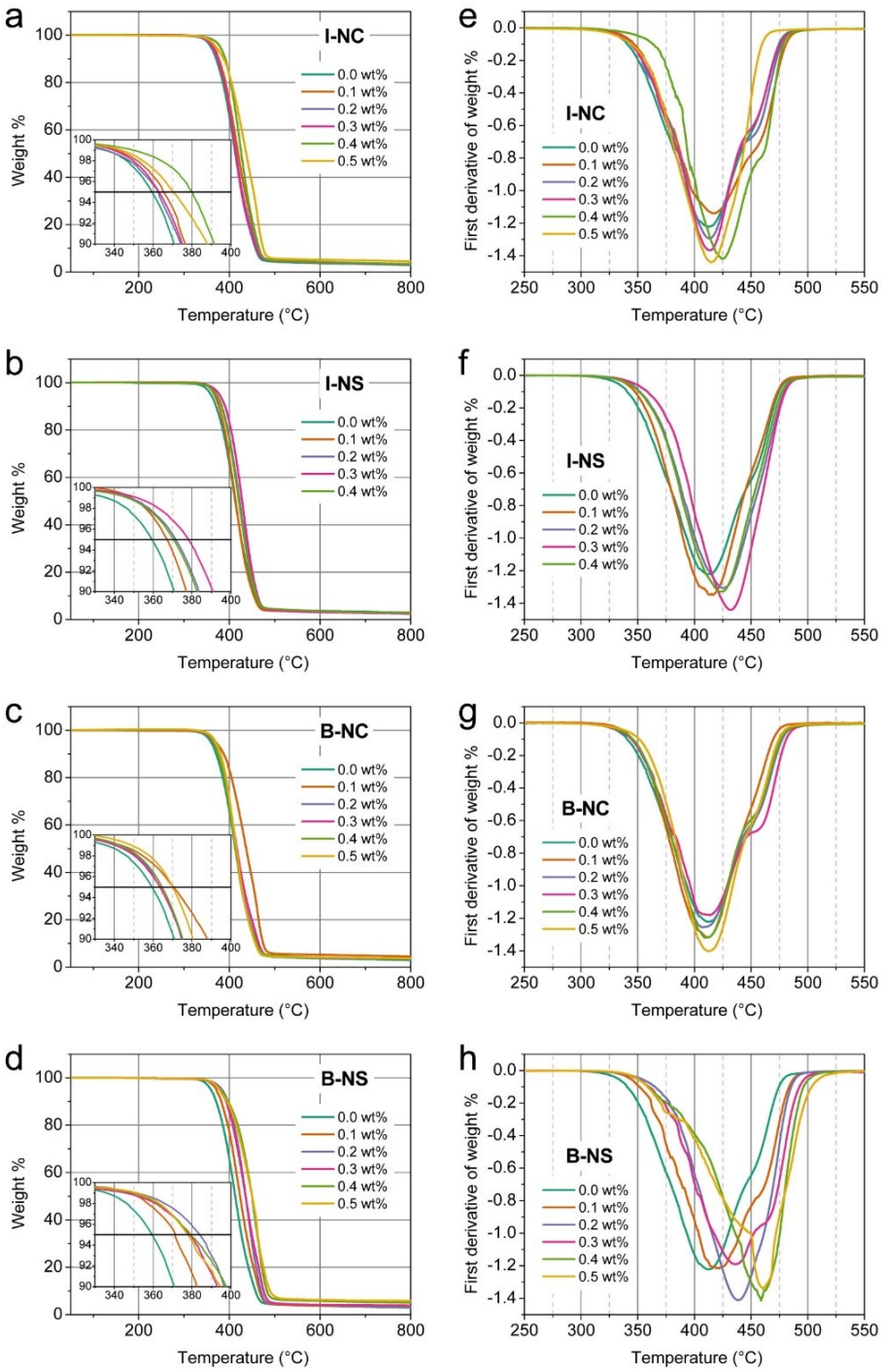

Fig. S7 Thermogravimetric analysis curves of (a) *in situ* Ny66/CNC (I-NC), (b) *in situ* Ny66/ CSW (I-NS), (c) solution-blended Ny66/CNC (B-NC), and (d) solution-blended Ny66/CSW (B-NS) nanocomposite films. Insets: magnified view of the onset thermal degradation. Corresponding differential thermogravimetric (DTG) curves of (e) I-NC, (f) I-NS, (g) B-NC, and (h) B-NS nanocomposite films.

The thermal degradation of pristine nylon 66 and its nanocomposite films was investigated by thermal gravimetric analysis (TGA). The results are shown in Fig. S7, and their degradation temperatures are given in Table S1. The degradation of the pristine film took place over the 350 to 500 °C range. The decomposition temperature for a 5% weight loss (T_{d5}) was ~359 °C and the maximum decomposition temperature (T_{max}) was ~408 °C; these obtained values are consistent with reported values.[38]

The sulfuric acid-treated cellulose nanocrystals (CNC) have been reported to exhibit two well-separated pyrolysis processes (one between 150 and 290 °C and the other between 320 and 500 °C),[39,40] whereas CSW is known to have one major weight loss decomposition beginning at above 200 °C and peaking at 350 °C.[41] The thermograms of all the composite films were similar to that of the pristine film, indicating no separate degradation stage of either CNC or CSW, regardless of the nanofiller loading level (Fig. S7). This suggests good dispersion and uniform distribution of the nanofiller within the polymer matrix. Although the thermal degradation regimes of both nanofillers are lower than that of the polymer, incorporation of the nanofiller into the polymer matrix even at a low concentration showed an improvement in the thermal stability of the resulting composites.

This thermal stability enhancement is likely attributed to the synergistic effects of filler-matrix interaction through hydrogen bonding or covalent linkage. Furthermore, these interactions were responsible for the uniform heat absorption and the higher energy input requirement for decomposition. They also reduced polymer molecular mobility and prevented the diffusion of formed volatile decomposition products, leading to improved thermal profiles of the composites.[42] Under the same composite synthesis method, CSW appeared to enhance the thermal stability of the composite films, better than that with CNC. An increase by at least by 4 °C of the T_{d5} of the nanocomposites was realized, along with an increase in the T_{max} values. Interestingly, B-NS samples experienced an unusual elevation in their T_{max}, reaching as high as 460 °C, 50 °C higher than that of the pristine film (Table S1), which is probably due to ionization of CSW by formic acid during the post-blending.[43] However, no remarkable correlation was found between the filler loading and the thermal properties of the composites because of the involvement of complicated energy dissipating mechanisms of the nanofillers.[44]

REFERENCES

1 Z. M. dos Santos, A. L. P. F. Caroni, M. R. Pereira, D. R. da Silva and J. L. C. Fonseca, *Carbohydr. Res.*, 2009, **344**, 2591–2595.

2 C. Lim, D. W. Lee, J. N. Israelachvili, Y. Jho and D. S. Hwang, *Carbohydr. Polym.*, 2015, **117**, 887–894.

3 A. C. Corrêa, E. de Morais Teixeira, V. B. Carmona, K. B. R. Teodoro, C. Ribeiro, L. H. C. Mattoso and J. M. Marconcini, *Cellulose*, 2014, **21**, 311–322.

4 H. Yousefian and D. Rodrigue, *Polym. Compos.*, 2016, **37**, 1473–1479.

5. S. Savetlana, L. Mulvaney-Johnson, T. Gough and A. Kelly, *Plast. Rubber Compos.*, 2018, **47**, 77–86.

6 P. A. de Arcaya, A. Retegi, A. Arbelaiz, J. M. Kenny and I. Mondragon, *Polym. Compos.*, 2009, **30**, 257–264.

7 H. Oliver-Ortega, L. A. Granda, F. X. Espinach, J. A. Mendez, F. Julian and P. Mutjé, *Compos. Sci. Technol.*, 2016, **132**, 123–130.

8 E. L. Papadopoulou, F. Pignatelli, S. Marras, L. Marini, A. Davis, A. Athanassiou and I. S. Bayer, *RSC Adv.*, 2016, **6**, 6823–6831.

9 M. M. Hossain, H. Shima, I. Lee and J. R. Hahn, *J. Appl. Polym. Sci.*, 2017, **134**, 45034.

10 X. Zhang, X. Fan, H. Li and C. Yan, *J. Mater. Chem.*, 2012, **22**, 24081–24091.

11 A. Dorigato and A. Pegoretti, *Polym. Eng. Sci.*, 2019, **59**, 198–205.

12 M. Kang, S. J. Myung and H.-J. Jin, *Polymer*, 2006, **47**, 3961–3966.

13 R. Sengupta, A. Ganguly, S. Sabharwal, T. K. Chaki and A. K. Bhowmick, *J. Mater. Sci.*, 2007, **42**, 923–934.

14 H. Xia, Q. Wang and G. Qiu, *Chem. Mater.*, 2003, **15**, 3879–3886.

15 W. D. Zhang, L. Shen, I. Y. Phang and T. Liu, *Macromolecules*, 2004, **37**, 256–259.

16 A. R. Bhattacharyya, P. Pötschke, L. Häußler and D. Fischer, *Macromol. Chem. Phys.*, 2005, **206**, 2084–2095.

17 M. Moniruzzaman, J. Chattopadhyay, W. E. Billups and K. I. Winey, *Nano Lett.*, 2007, **7**, 1178–1185.

18 S.-H. Wu, F.-Y. Wang, C.-C. M. Ma, W.-C. Chang, C.-T. Kuo, H.-C. Kuan and W.-J. Chen, *Mater. Lett.*, 2001, **49**, 327–333.

19 L. Shen, I. Y. Phang, L. Chen, T. Liu and K. Zeng, *Polymer*, 2004, **45**, 3341–3349.

20 A. Ranade, N. A. D'Souza, B. Gnade and A. Dharia, *J. Plast. Film Sheeting*, 2003, **19**, 271–285.

21 W. Shao, Q. Wang, F. Wang and Y. Chen, *J. Polym. Sci. Part B: Polym. Phys.*, 2006, **44**, 249–255.

22 K. Hedicke-Höchstötter, G. T. Lim and V. Altstädt, *Compos. Sci. Technol.*, 2009, **69**, 330–334.

23 K. Prashantha, M.-F. Lacrampe and P. Krawczak, *J. Appl. Polym. Sci.*, 2013, **130**, 313–321.

24 X. Xu, B. Li, H. Lu, Z. Zhang and H. Wang, *Appl. Surf. Sci.*, 2007, **254**, 1456–1462.

25 C. G. Cannon, *Spectrochim. Acta*, 1960, **16**, 302–319.

26 S. J. Cooper, M. Coogan, N. Everall and I. Priestnall, *Polymer*, 2001, **42**, 10119–10132.

27 Y. Ma, T. Zhou, G. Su, Y. Li and A. Zhang, *RSC Adv.*, 2016, **6**, 87405–87415.

28 I. Sandeman and H. W. Thompson, *Proc. R. Soc. A: Math. Phy. Eng. Sci.*, 1955, **232**, 105–113.

29 I. Matsubara and J. H. Magill, *Polymer*, 1966, **7**, 199–215.

30 D. Galimberti, C. Quarti, A. Milani, L. Brambilla, B. Civalleri and C. Castiglioni, *Vib. Spectrosc.*, 2013, **66**, 83–92.

31 C. G. Cannon and P. H. Harris, *J. Macromol. Sci. Part B: Phys.*, 1969, **3**, 357–364.

32 J. L. Koenig and M. C. Agboatwalla, *J. Macromol. Sci. Part B: Phys.*, 1968, **2**, 391–420.

33 N. Vasanthan, N. S. Murthy and R. G. Bray, *Macromolecules*, 1998, **31**, 8433–8435.

34 N. Vasanthan and D. R. Salem, *J. Polym. Sci., Part B: Polym. Phys.*, 2000, **38**, 516–524.

35 N. Vasanthan and D. R. Salem, *Mater. Res. Innovations*, 2001, **4**, 155–160.

36 D. Garcia and H. W. Starkweather Jr., *J. Polym. Sci., Polym. Phys. Ed.*, 1985, **23**, 537–555.

37 E. Chi, M. An, G. Yao, F. Tian and Z. Wang, *Crystals*, 2017, **7**, 384.

38 A. Attanasio, I. S. Bayer, R. Ruffilli, F. Ayadi and A. Athanassiou, *ACS Appl. Mater. Interfaces*, 2013, **5**, 5717–5726.

39 J. Gong, J. Li, J. Xu, Z. Xiang and L. Mo, *RSC Adv.*, 2017, **7**, 33486–33493.

40 N. Wang, E. Ding and R. Cheng, *Polymer*, 2007, **48**, 3486–3493.

41 A. G. B. Pereira, E. C. Muniz and Y.-L. Hsieh, *Carbohydr. Polym.*, 2014, **107**, 158–166.

42 D. Bikiaris, *Thermochim. Acta*, 2011, **523**, 25–45.

43 M. Nagalakshmaiah, N. El Kissi and A. Dufresne, *ACS Appl. Mater. Interfaces*, 2016, **8**, 8755–8764.

44 G.-m. Wu, D. Liu, G.-f. Liu, J. Chen, S.-p. Huo and Z.-w. Kong, *Carbohydr. Polym.*, 2015, **127**, 229–235.